Investigation by laser Doppler anemometry of the turbulent flow around cylindrical obstacles on a rough surface

F. K. Lim* and A. K. Lewkowicz†

Mean flow and turbulence measurements were made in the separated region and around a vertical cylindrical obstacle submerged in a turbulent boundary layer and mounted on an irregularly rough surface. Solid cylinders and cylinders with a concentric cavity at the top were used as the isolated obstacles. The experiment demonstrated that the presence of a cavity enhanced turbulent stresses just above the cylinder. Double-peaked turbulent stress profiles could be found in the separated zone, which could be interpreted in terms of a double-vortex model.

Keywords: *turbulence, vortex, roughness, laser Doppler anemometry*

Accurate data of the flow in the separated region past surface-mounted obstacles is still substantially incomplete. Whilst the downstream recirculation behind two-dimensional obstacles has been studied by Crabb, Durao and Whitelaw[1], Durst and Rastogi[2] and others, a three-dimensional near wake flow behind a cube has been reported in some detail only by Castro and Robins[3]. Other fundamental geometries of surface-mounted obstacles also require attention because of their practical applications and significance. Such a geometry of interest to the present authors was a vertical circular cylinder with and without a concentric cavity in its top surface (hollow cylinder).

In this investigation the obstacle was fully submerged in a turbulent boundary layer with zero pressure gradient developing on an irregularly rough flat surface. Its height was about a third of the boundary layer absolute thickness. A noninvasive laser Doppler anemometry (LDA) technique was employed to measure the mean and fluctuating velocities around the obstacle, with main emphasis on the separated region past it. This technique is advantageous in many ways but chiefly because it dispenses with the necessity of physically entering the sensitive region of separated flow and thus interfering with its natural unstable flow structure. The depth of the roof cavity in the hollow cylinder could be varied and the flat surface on which the obstacles were mounted was in all cases covered with an irregular, but uniformly distributed, roughness. Thus the created flow model was that of an isolated 'macroroughness' element (the obstacle) interacting with the boundary layer flow on a background 'microroughness'.

* Senior Naval Architect, John Brown Offshore, John Brown House, 20 Eastbourne Terrace, London W2 6LE, UK. Formerly Research Student, Department of Mechanical Engineering, University of Liverpool, Liverpool L69 3BX, UK
† Senior Lecturer, Department of Mechanical Engineering, University of Liverpool, Liverpool L69 3BX, UK
Received 14 June 1985 and accepted for publication in final form on 18 November 1985

Flows of this nature occur frequently in real situations, eg barnacle shells or structural surface elements on a rough ship-hull; round buildings, cooling towers or storage tanks on the Earth's surface, etc. An additional objective of this exercise was to provide a further test case for complex computational schemes, in which the isolated obstacle would be of a simple, fundamental geometry.

Experimental arrangements

Fig 1 shows how the model obstacles, all 15 mm in height and diameter, were subjected to a fully established turbulent boundary layer flow without longitudinal pressure gradient. To make the boundary layer absolute thickness about three times the obstacle height at the obstacle location, fixed at 1580 mm downstream from the leading edge of the plate, a vertical wire fence was erected near the leading edge. The fence was 60 mm behind the edge and was made of 1.6 mm wire; it consisted of a single wire fixed to the rough surface (spanning 800 mm width of the plate) to which were attached at equal 12 mm intervals vertical struts also 12 mm high. All obstacle cavities, when used, were cylindrically coaxial and 9 mm in diameter. Two top cavity depths were studied in addition to the solid obstacle: a half-height cavity and a full-height cavity.

The background microroughness was created by means of Grade 16 floor abrasive paper of about 1 mm average height (ten-point height TPH, considering a typical two-dimensional roughness profile). In order to maintain the boundary layer development under constant longitudinal pressure, the elastic ceiling of the wind-tunnel, 240 mm above the plate, was suitably adjusted and the static pressure distribution along the plate centreline carefully checked.

A single-channel LDA system[4] was used to monitor the flow field; it was based on a 10 mW He–Ne laser and a counter processor and operated in a forward scattering dual beam mode. Frequency shift facility (Bragg cell) was incorporated to allow measurement of the

negative velocities. Both longitudinal and transverse velocity components could be measured owing to the possibility of rotating the transmitting optics assembly about its optical axis. Turbulent normal and shear stress components could thus be evaluated by invoking the same technique which is used to measure the said quantities by a single, slanted hot wire. Since two or more consecutive measurements separated by beam rotation are taken in this case, it is a basic requirement that the flow be stationary. Two consecutive measurements are needed for the normal transverse turbulent stresses and from three such measurements turbulent shear stresses can be deduced. Unfortunately, the optics rotation in the forward scattered mode prevents the transverse velocity components from being accessible closer than 8 mm from the wall. Of course, this limitation was due to the fact that the laser beam was directed at the flow field and the scattered light collected through two respective glass windows in the side walls of the wind-tunnel working section. Whilst the experimental accuracy of the longitudinal mean velocity and normal turbulent stress was quite good, being 2% or better, experimental errors of up to 12% should be reckoned with in some of the turbulent transverse and shear stresses.

Special attention had to be paid to feeding the wind-tunnel flow with the right kind and amount of seeding essential to securing optimum LDA signal strength and quality to provide a sufficiently fast rate of data sampling. A commercial smoke generator vapourizing Shell Ordina 17 mineral oil served this purpose well but a considerable trial-and-error learning period could not be avoided.

Characteristics of the undisturbed boundary layer flow

Measurements were carried out at two different free stream velocities, $U_\infty = 6$ and 20 m/s, for the mean velocity profiles of the boundary layer flow undisturbed by the macroroughness obstacle.

Analysis of the velocity profiles reveals that if the classical law of the wall for the turbulent boundary layer on a smooth wall is assumed (with its constituent constants 0.4 and 5.0), the background roughness manifests itself by the following values of the roughness function: at $U_\infty = 6$ m/s, Nikuradse's $\chi = 6.17$ and downward velocity shift $\Delta U/u_0 = 6.44$; at $U_\infty = 20$ m/s, $\chi = 4.75$ and $\Delta U/u_0 = 11.00$. The behaviour of this roughness function, published in full by Lim[5] in terms of the roughness Reynolds number, hu_0/ν, where h is the centreline average (CLA) roughness height, indicates that at $U_\infty = 6$ m/s the flow regime in the undisturbed boundary layer has an intermediately rough nature whereas for $U_\infty = 20$ m/s it is fully rough.

Turbulent normal and shear stresses, $\overline{u^2}$, $\overline{v^2}$ and $-\overline{uv}$, are shown in Fig 2, where u_0 and δ, the absolute boundary layer thickness, are used to normalize the stresses and y, respectively.

Klebanoff's[6] measurements on a smooth wall were used to demonstrate the effect of wall roughness on the

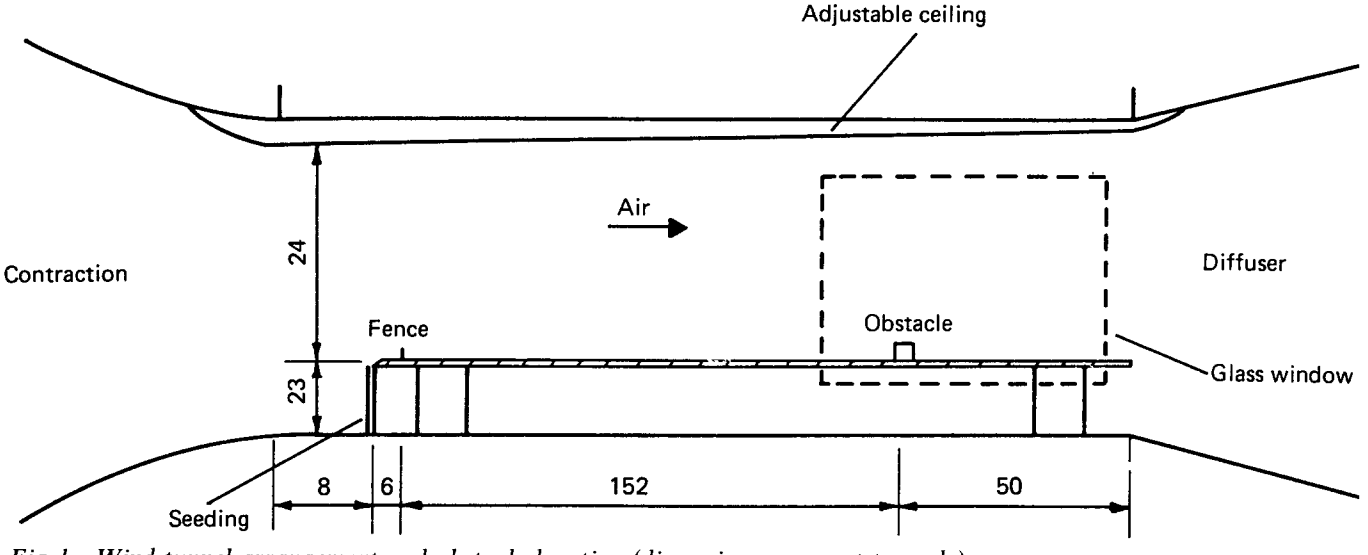

Fig 1 Wind-tunnel arrangement and obstacle location (dimensions: cm; not to scale)

Notation

d_c	Depth of the cylinder-top cavity
h	Background microroughness height
H	Cylinder height
u,v	Fluctuating velocity components in x and y directions, respectively
u_0	Friction velocity, $\sqrt{\tau_0/\rho}$
U,V	Mean velocities in x and y directions, respectively
U_∞	Free stream mean velocity
$\Delta U/u_0$	Dimensionless velocity shift in law of the wall
x	Coordinate in longitudinal direction measured from the back of the cylinder
y	Coordinate in vertical direction measured from the plane wall
z	Coordinate in transverse direction measured from the plane of symmetry
δ	Boundary layer absolute thickness (at $U = 0.995U_\infty$)
ν	Kinematic viscosity of air
ρ	Density of air
τ_0	Wall shear stress
χ	Nikuradse's roughness function

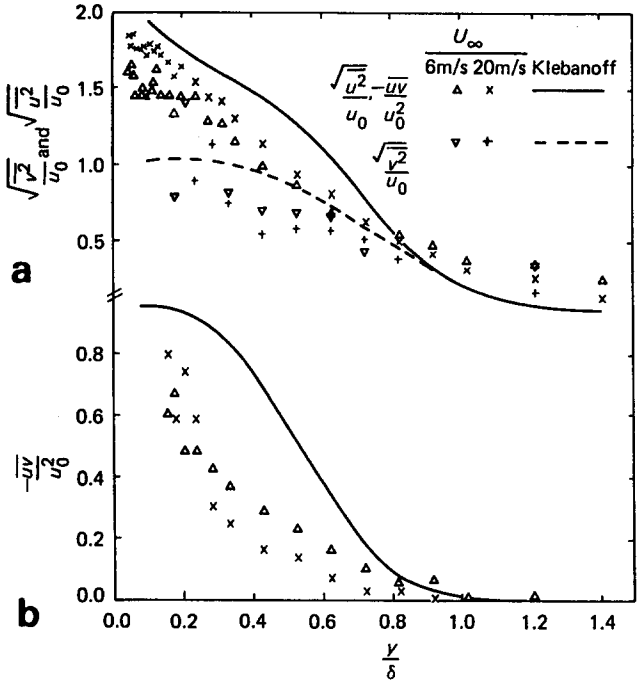

Fig 2 Turbulent normal and shear stresses on flat plate with irregular background roughness

turbulent stresses in the undisturbed boundary layer. Almost a threefold reduction in $-\overline{uv}/u_0^2$ around $0.25<(y/\delta)<0.45$ is seen in Fig 2(b) to be caused by the roughness. Smaller-magnitude, but equally noticeable, reductions in $\overline{u^2}$ and $\overline{v^2}$ in the region are shown by Fig 2(a). Such reductions in the turbulent stresses are now well documented for almost all wall-bounded turbulent shear flows. Probably the first to point out their existence were Townes, Gow, Powe and Weber[7].

Detailed characteristics of the undisturbed boundary layer flow are listed here as Table 1 and some key statistical properties of the background roughness are given further as Table 2.

Flow in the vicinity of the obstacle

Mean flow

Although the mean flow velocities were measured in different spanwise planes, the present results are restricted mainly to those in the central plane, $z=0$, where z is the spanwise coordinate normal to the plane of the drawing in Fig 1. A comprehensive account of the measurements actually taken can be found in Lim[5].

Mean velocity vectors around a solid cylinder in the $z=0$ plane are shown in Fig 3 for different x/H stations and within the range $-2<x/H<5$, where H is the obstacle height and positive x points in the direction of flow, with $x=0$ coinciding with the downstream intersection of the cylinder side surface and the $z=0$ plane. These vectors are given for both $U_\infty=6$ and 20 m/s. No low frequency flow unsteadiness was ever detected during any of these measurements thus confirming the assumption of stationary flow. The size of the recirculating flow region caused by the obstacle is more extensive at the lower flow Reynolds number $(U_\infty H/\nu)=5990$.

Turbulent stresses

Results of the measurements of the longitudinal and transverse turbulent normal stresses are presented in Fig 4. Their distributions in the central plane, $z=0$, are plotted for $U_\infty=6$ and 20 m/s in Figs 4(a) and 4(b), respectively; there follow Figs 4(c) through 4(f) illustrating the spanwise variation of the stresses at $U_\infty=20$ m/s in planes $z=0.33H$, $0.67H$, $1.00H$ and $2.33H$. An alternative presentation of the spanwise distribution of the longitudinal stresses is given in Fig 5; it is a planner plot of the stresses at $y=0.52H$ and $0.95H$. Both normal stresses clearly peak at the obstacle roof level in the downstream separated flow region. These peaks become substantially 'diffused' for $x>5H$ and $z>H$.

Turbulent normal stresses above the solid and hollow cylindrical obstacles are shown in Fig 6, which indicates that the cavity noticeably enhances the normal stresses near the top of the obstacle and possibly promotes earlier peaking of the stresses downstream of the obstacle.

Essentially similar in character, the behaviour of the turbulent shear stresses is given in Fig 7. The shear stress peaks downstream of the rear roof trailing edge are here in places relatively very strong (reaching some ten times their neighbouring base value at $z=0$; $x=0.67H$ for $U_\infty=20$ m/s). Measured but not presented, turbulent shear stresses just above the obstacle roof are also significantly amplified by the presence of the top cavity in the obstacle.

Flow visualization

A lamp-black surface flow visualization was carried out on the side surface of the cylindrical obstacle. The resultant surface flow pattern, reproduced in Fig 8,

Table 1 Undisturbed boundary layer characteristics

Parameters	U_∞ 6 m/s	U_∞ 20 m/s
Friction velocity u_0, m/s	0.349	1.285
Velocity shift $\Delta U/u_0$	6.44	11.00
Cole's wake strength parameter Π	0.301	0.273
Absolute thickness $\delta_{0.995U_\infty}$, mm	51.1	50.6
Displacement thickness δ^*, mm	9.01	9.13
Momentum thickness θ, mm	5.73	5.71
Reynolds number $U_\infty\theta/\nu$	2289	7583
Obstacle Reynolds number $U_\infty H/\nu$	5990	19940

Table 2 Statistical characteristics of background roughness profile

Parameters	Values[a]
Peak-to-valley height	1270
Ten-point height (TPH)	1002
Centreline average height (CLA)	134
Root-mean-square height	191
Average slope, degrees	14.8
Skewness	0.70
Kurtosis	4.09

[a] All length dimensions in μm

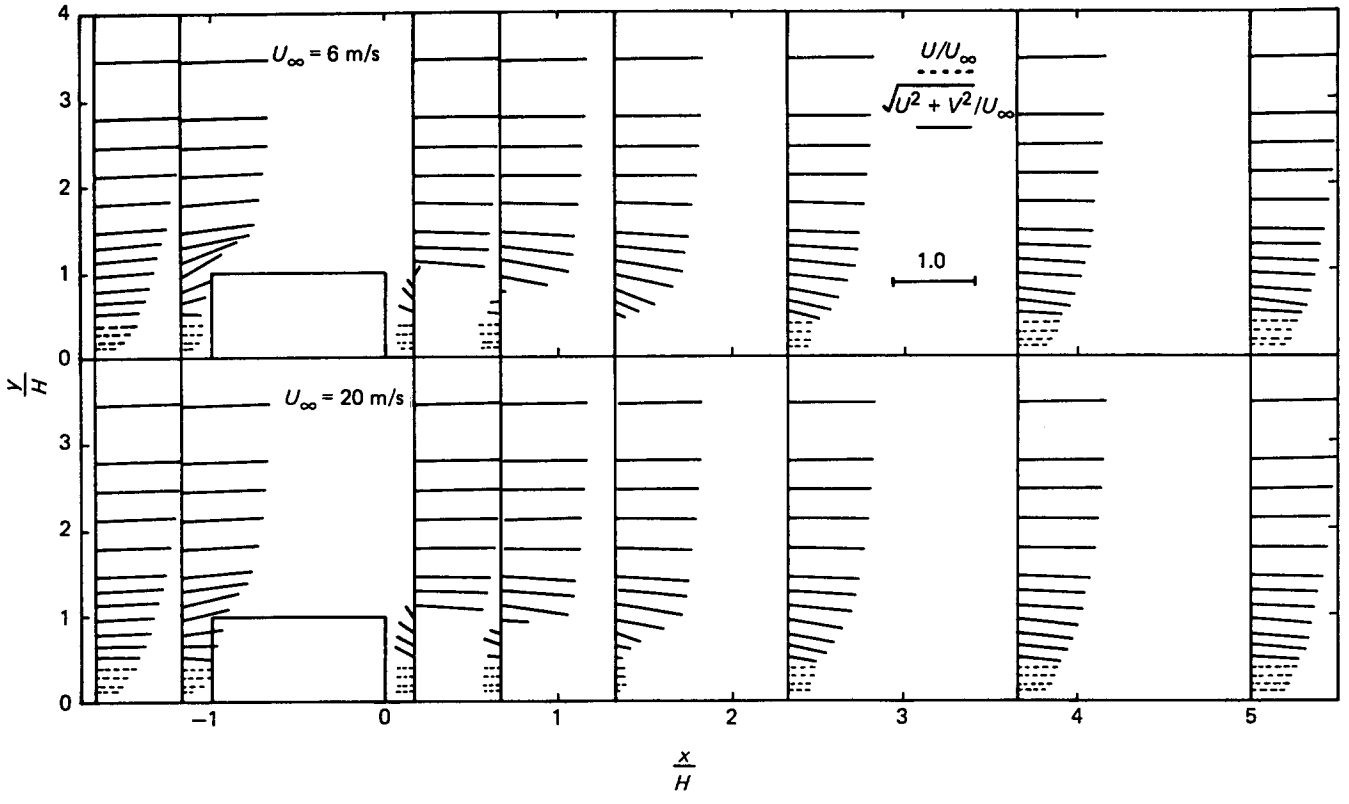

Fig 3 Mean velocity vectors around cylinder in plane of symmetry

portrays clearly both the front and rear stagnation lines on the cylinder together with the line of rear separation. On either side of the rear stagnation line, near the bottom of the obstacle, there are clear traces of the separation vortex loop characterizing the flow in the separation bubble behind a surface-mounted cylindrical obstacle.

Discussion of results

As expected, the cylinder on the rough surface deflects the incident flow upwards and sideways. The flow separates from the top and sides of the cylinder, forming a complex recirculation flow region. Although it was not intended to fully monitor the flow recovery past the obstacle, the distortion of the boundary layer flow caused by it can be seen to have almost died out at the farthest downstream measurement station, ie at $x=5H$ in this investigation. This agrees with the measurements of Castro and Robins[3] who observed that the wake behind a wall-mounted cube vanishes completely within about six cube heights when it is fully submerged in the boundary layer. The extent of the recirculating flow zone, domainted by the vortex loop whose origin is seen in Fig 8, is estimated on the basis of the present LDA mean velocity and turbulence measurements to be about one cylinder height long (see Fig 4). The said vortex should not be confused with the well-known horseshoe vortex always present around surface-mounted obstacles, the evidence of which is also seen in Fig 8. Its pattern may be detected there near the bottom line. The twin vortex trace clearly visible at the rear of the cylinder is a mark of a loop vortex entirely enclosed by the separation bubble. The plan view of the longitudinal normal stresses (Fig 5) shows stress peaks in the z direction which could be interpreted as coinciding with the demarcation lines between the inner loop vortex and the horseshoe vortex. This view may be reinforced by the fact that at $y=0.52H$ the stress prfiles show slightly stronger peaks than at $y=0.95H$. Additionally, one notices that the higher Reynolds number flow ($U_\infty=20$ m/s) has the ability to confine the separation bubble to a narrower region (in the z direction) than the slower flow ($U_\infty=6$ m/s).

The normal and shear stress distributions in the $z=0$ plane (Figs 4 and 7, respectively) are primarily indicative of the consequences of flow separation taking place on the top of the cylinder, and its interaction with the main separation bubble behind the obstacle. Examining carefully the turbulent stress distributions one notices a curious phenomenon: for $x>0.67H$ all turbulent stresses develop a sharp peak (maximum) whereas measurements taken at $x=0.17H$ show no, or little, evidence of such peaks even though they are closer to the obstacle. One finds it difficult to explain this feature adequately and a further investigation is needed to discover the reasons for this sudden and localized source of turbulence production. Castro and Robins[3] also measured a comparable turbulent stress peak behind a surface-mounted cube in a turbulent boundary layer, and their measurements taken at $x=0.5H$ are roughly comparable with the present measurements at $x=0.67H$. The stress peaks in the $z=0$ plane tend to decay with x and, as already mentioned, at $x=5H$ the stress distributions are close to those of the undisturbed boundary layer flow. An interesting observation can be made when examining the stress distributions with the effect of the top cavity in the cylinder (Fig 6). It appears

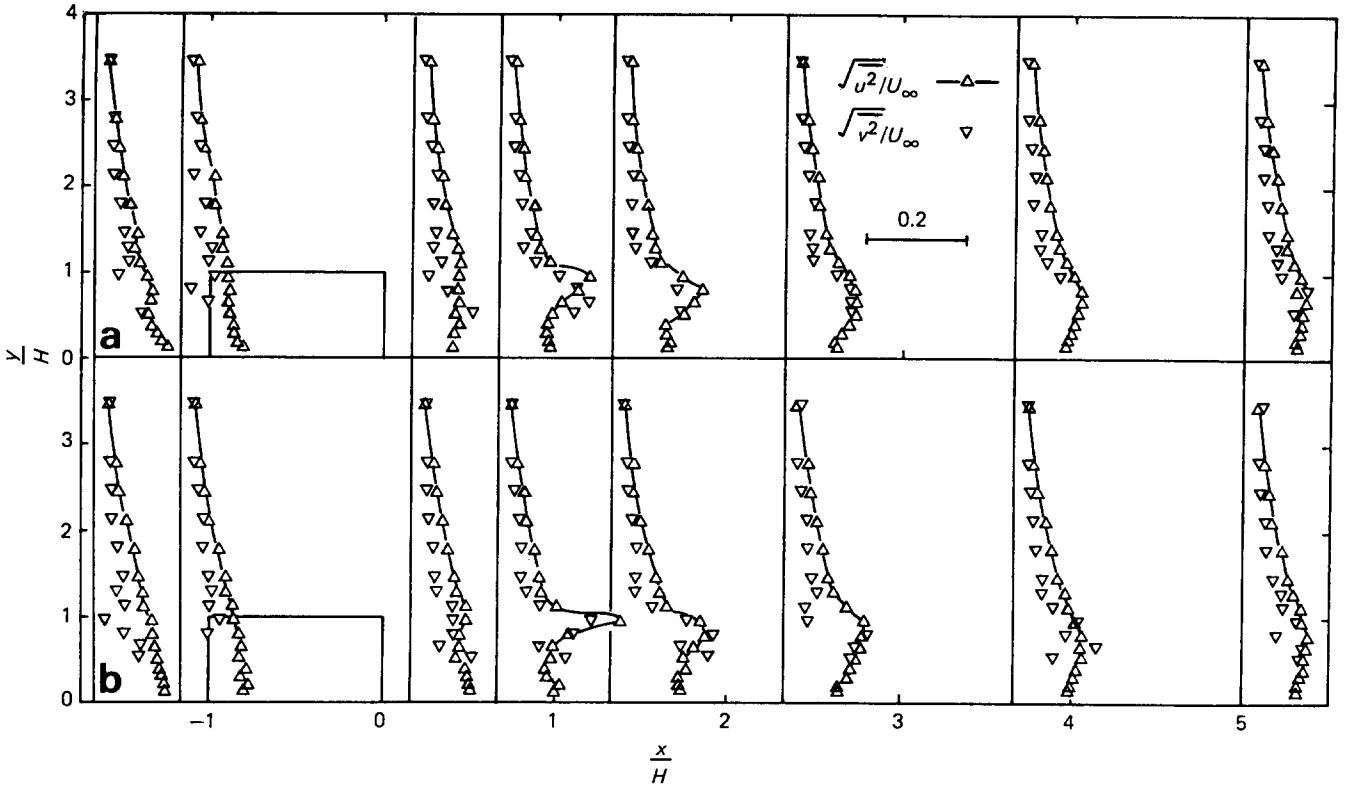

Fig 4 Turbulent normal stresses around cylinder in plane of symmetry: (a) $U_\infty = 6$ m/s, $z = 0$; (b) $U_\infty = 20$ m/s, $z = 0$; (c) $U_\infty = 20$ m/s, $z = 0.33H$; (d) $U_\infty = 20$ m/s, $z = 0.67H$; (e) $U_\infty = 20$ m/s, $z = H$; (f) $U_\infty = 20$ m/s, $z = 2.33H$

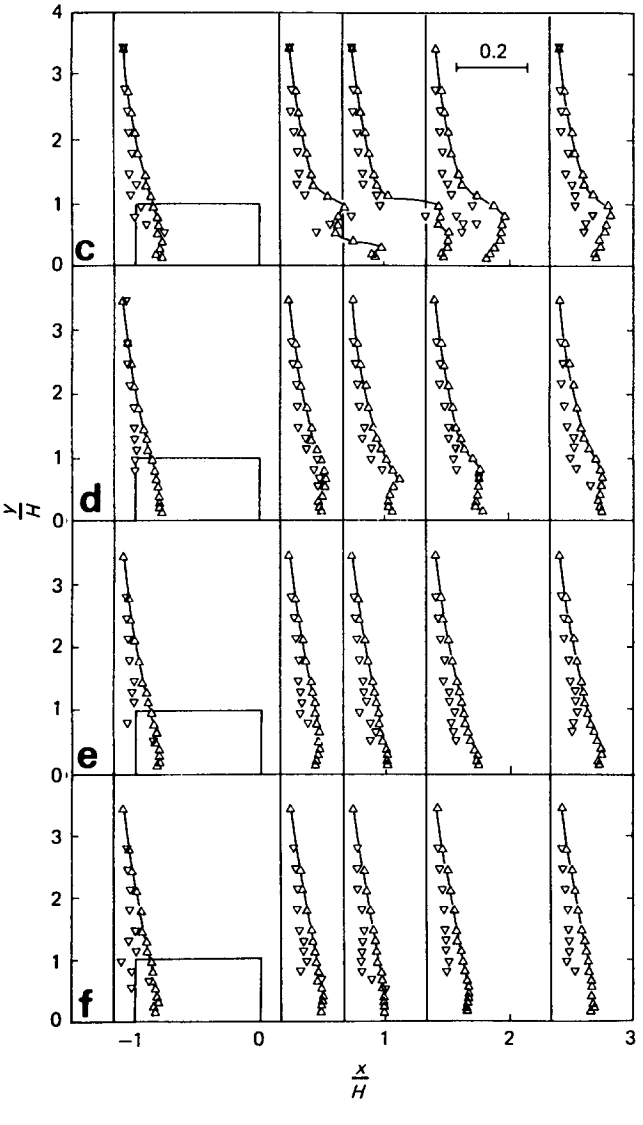

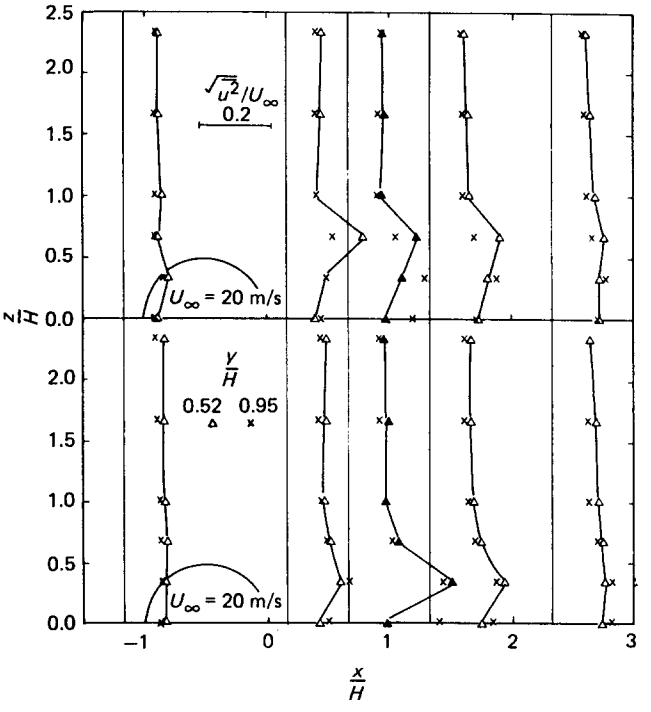

Fig 5 Spanwise variation of longitudinal turbulent normal stresses

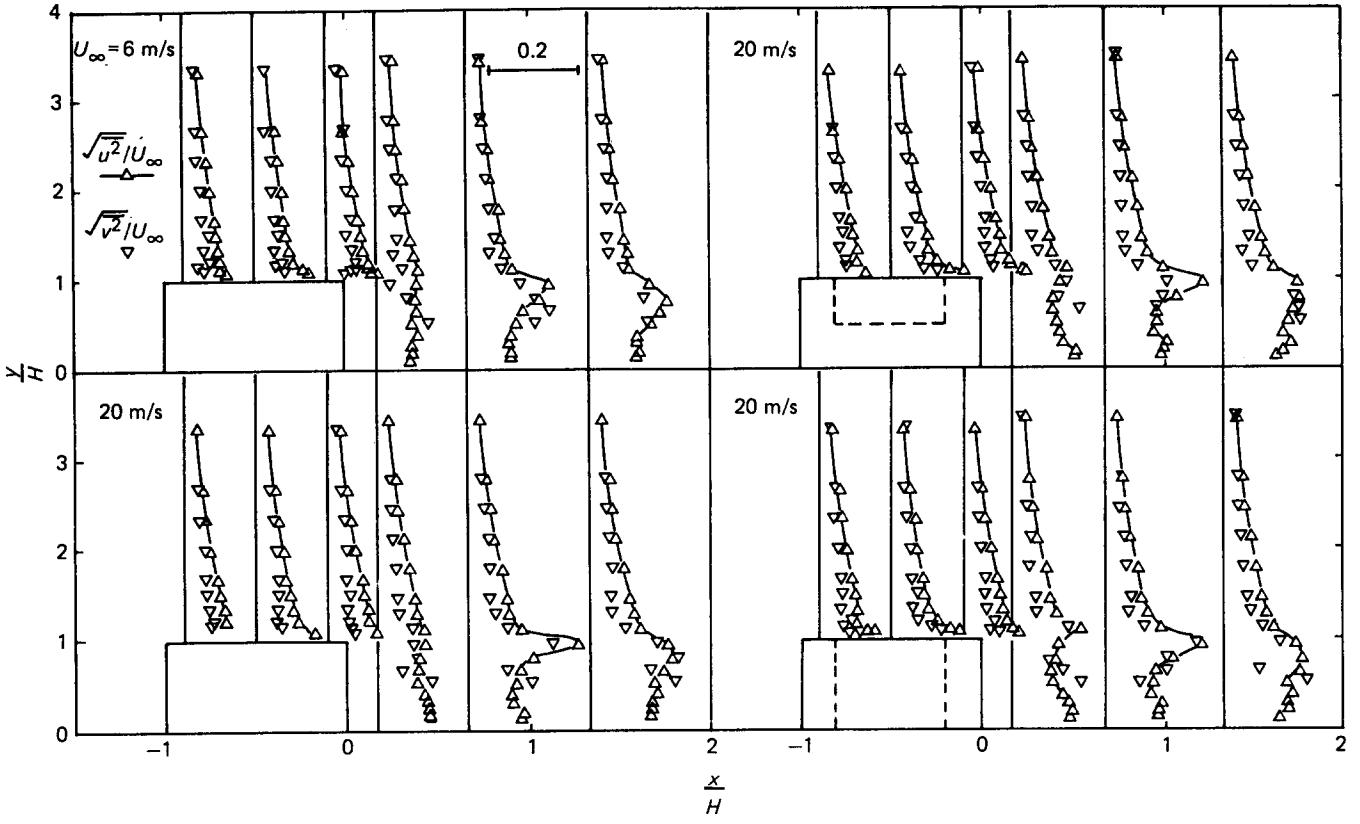

Fig 6 Turbulent normal stresses above cylinder in plane of symmetry

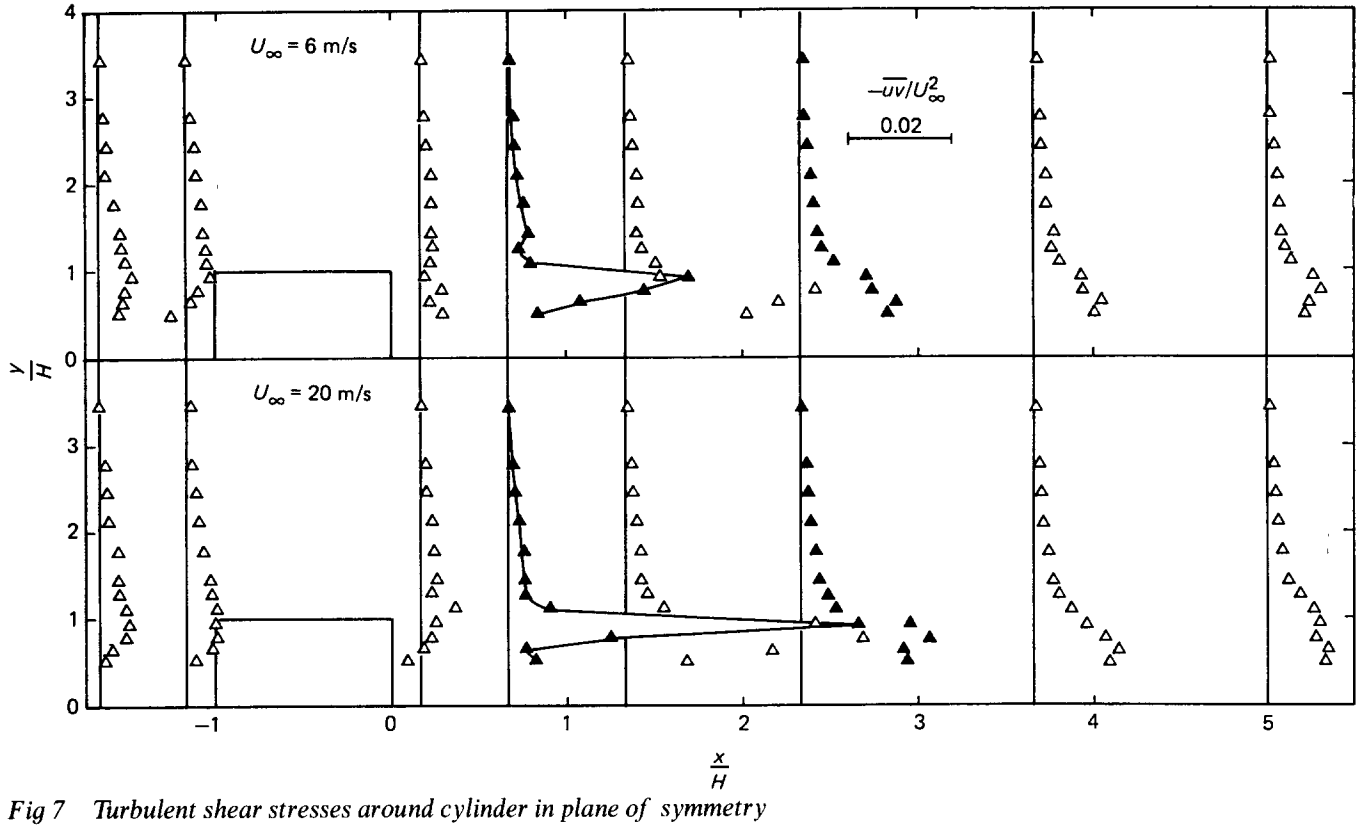

Fig 7 Turbulent shear stresses around cylinder in plane of symmetry

that with the cavity present the stress peak occurs earlier—at $x=0.17H$. There is also weak evidence that this occurrence is intensified with the depth of cavity. Also the secondary flow inside the cavity seems to induce stronger turbulent stresses just at the top of the cylinder (by up to 30%). Furthermore, during the experiments, the cavity has been observed to displace upward the mean flow along the cylinder centreline. A plausible explanation of this phenomenon could be the interaction of the mean flow with the secondary flow inside the cavity resulting in a bulged neutral velocity surface above the top of the cylinder.

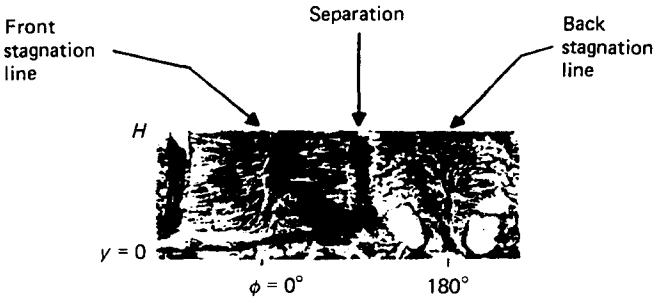

Fig 8 Surface flow pattern on cylinder

One comes across further evidence of the inner loop vortex when one scrutinizes the turbulent normal and shear stress distributions away from the central plane $z=0$. The measurements taken at $z=0.33H$ (Fig 4(c)) show a double peak in the normal stress distributions starting from $x \geqslant 0.17H$ but the peaks tend to merge for $x > 1.3H$ and thereafter diffuse in the usual way. No such double peak has been detected experimentally for the shear stress distributions but these measurements, as explained before, could not be taken close to the wall. Likewise, turbulent stress measurements taken further out sideways, at $z=0.67H$, show the double peak tendency but the lower peak is now substantially weaker. This is likely to be representative of the coexistence there of the loop and horseshoe vortices. At $z=0.33H$ one most likely picks up signals close to the core of the loop vortex, whereas at $z=0.67H$ the influence of the loop vortex becomes weak and the horseshoe vortex begins to dominate.

One must realize that these measurements were taken around an obstacle mounted on an irregularly rough surface and that the effect of the background roughness could be pronounced. Strictly the work ought to be repeated with the same cylinder mounted on a smooth surface. This would enable one to quantify the effect of the background roughness on all the above-discussed quantities.

Conclusion

An LDA system was successfully employed in an experimental investigation of a complex turbulent shear flow past a cylindrical obstacle mounted on a rough surface. The noninvasive nature of the technique and its linear response together with the ability of monitoring reverse flow components enabled a detailed survey of the separated flow region past the obstacle to be carried out in terms of the mean flow and turbulent property characteristics. Experimental accuracy of some 2% was achieved in measuring the mean flow velocities and longitudinal turbulent normal stresses. Turbulent transverse normal and shear stresses were measured to within 12% (in worst cases). Another novel element in this experiment is the fact that the obstacle flow was affected by the uniformly distributed irregular roughness on the surface on which the obstacle was mounted. The flow properties in the separated zone are interpreted in terms of a double vortex model involving mutual interaction of the well-known horseshoe vortex and a loop vortex attached to the rear of the obstacle (Fig 8) and embedded entirely within the separation bubble.

References

1. **Crabb D., Durao D. F. G. and Whitelaw J. H.** Velocity characteristics in the vicinity of a two-dimensional rib. *Proc. Fourth Brasilian Congress of Applied Mechanics, 1977, 415*
2. **Durst F. and Rastogi A. K.** Theoretical and experimental investigations of turbulent flows with separation. *Turbulent Shear Flow I, selected papers from the First Symp. on Turbulent Shear Flow, 1979, Springer-Verlag*
3. **Castro I. P. and Robins A. G.** The flow around a surface mounted cube in uniform and turbulent streams. *J. Fluid Mech., 1977,* **79**, *307*
4. **Lim F. K. and Lewkowicz A. K.** LDA system in the Liverpool University Aero-Laboratory. *Proc. Colloqu. on Applications of LDA Counter Systems, Dec. 1983, Durham University, UK*
5. **Lim F. K.** Turbulent shear flows on rough walls with isolated elements or controlled texture. *PhD Thesis, 1983, University of Liverpool*
6. **Klebanoff P. S.** Characteristics of turbulence in a boundary layer with zero pressure gradient. *NACA TN 3178, 1954*
7. **Townes H. W., Gow J. L., Powe R. E. and Weber N.** Turbulent flow in smooth and rough pipes. *J. Basic Eng., Trans. ASME, 1972,* **94**, *353*